

---

# A toolbox to quickly prepare flood inundation models for LISFLOOD-FP simulations

---

Jeison Sosa (1), Chris Sampson (1,2), Andy Smith (1,2), Jeff Neal (1,2), Paul Bates (1,2)

(1) School of Geographical Sciences, University of Bristol, Bristol, BS8 1SS, UK

(2) Fathom Ltd., Engine Shed, Temple Meads, Bristol, BS1 6QH, UK

## Corresponding author

Jeison Sosa

School of Geographical Sciences

University of Bristol

Bristol, UK

Tel: +44 7460 807038

E-mail: [j.sosa@bristol.ac.uk](mailto:j.sosa@bristol.ac.uk)

## Abstract

Hydrodynamic floodplain inundation models have been popular for many years and used extensively in engineering applications. Continental scale flood studies are now achievable using such models due to the development of terrain elevation, hydrography and river width datasets with global coverage. However, deploying flood models at any scale is time-consuming since input data needs to be processed from different sources. Here we present LFPtools, which is an open-source Python package which encompasses most commonly used methods to prepare input data for large scale flood inundation studies using the LISFLOOD-FP hydrodynamic model. LFPtools performance was verified over the Severn basin in the UK where a 1 km flood inundation model was built within 1.45 mins. Outputs of the test case were compared with the official flood extent footprint of a real event and satisfactory model performance was obtained: Hit rate=0.79, False alarm ratio=0.24 and Critical success index=0.63.

## Keywords

Large-scale, continental-scale, modelling, toolbox, hydraulics, flood, LISFLOOD-FP, Python

40

41 **Highlights**

- 42 • LFPtools provides data processing methods to deploy LISFLOOD-FP models.
- 43 • LFPtools is written in way that more complex methods can be easily added.
- 44 • LFPtools can be used within a sensitivity analysis framework.
- 45 • LFPtools is intended for both non-specialist and experienced flood modellers.

46

47 **Software availability**

48 The toolbox developed in this research is written in Python and built on top of GDAL  
49 (<https://www.gdal.org>), Cython (<http://cython.org/>), Pandas (<https://pandas.pydata.org/>), Numpy  
50 (<http://www.numpy.org/>), xarray (<http://xarray.pydata.org>) and TauDEM  
51 (<http://hydrology.usu.edu/taudem/>). Code and installation instruction are available at  
52 <https://github.com/jsosa/LFPtools>. The toolbox is distributed under the 3-Clause BSD license.

53

54

55

## 56 **1 Introduction**

57

58 Hydrodynamic models designed to simulate floodplain inundation have been popular for many years  
59 and are widely used in engineering applications. These models, such as TUFLOW (Syme, 1991),  
60 JFLOW (Bradbrook et al., 2004), TRENT (Villanueva and Wright, 2006) and LISFLOOD-FP (Bates et  
61 al., 2010), route water through channels and floodplains following shallow water flow theory.

62

63 Global to continental scale flood studies are being used for insurers, multi-national corporations, NGOs  
64 and national governments. They have been made possible as a result of the appearance of global  
65 coverage datasets of terrain elevation (Farr et al., 2007; Tadono et al., 2015; Yamazaki et al., 2017;  
66 Rizzoli et al., 2017, Wessel et al., 2018), hydrography (Lehner et al., 2008; Yamazaki et al., 2019) and  
67 river width (Andreadis et al., 2013; Yamazaki et al., 2014; Allen and Pavelsky, 2018). These data sets,  
68 coupled with the parallel development of efficient two-dimensional flood models (Bates et al., 2010,  
69 Neal et al., 2012; Sanders et al., 2010) and advances in computational power (Neal et al., 2018; Lamb  
70 et al., 2009), have led to the implementation of flood inundation studies in data-sparse areas around  
71 the world at very high resolutions ( $10^2$ - $10^3$  m). As consequence, a variety of applications involving flood  
72 hydrodynamic variables —flood extent, water depth, flow velocity, flow discharge— have been explored  
73 (Winsemius et al., 2013; Sampson et al., 2015; Wing et al., 2018; Dottori et al., 2017; Alfieri et al., 2018;  
74 Schumann et al., 2016; Lu et al., 2016)

75

76 Building a flood model can be time-consuming since input data need to be processed from a variety  
77 different sources and adapted to a particular user's problem. The increasing quantity, complexity and  
78 resolution of useful datasets imparts an ever-growing burden of knowledge on model developers.  
79 Furthermore, the frequent update cycles of some datasets can cause module builds to go out of date  
80 quickly. Therefore, developing a flood inundation model requires a high level of skill in handling  
81 geographical information using Graphical User Interface (GUI) driven software packages such as  
82 ArcGIS and QGIS. These present a workable solution for the treatment of data, but typically only at  
83 small-scales due to their high demands for computing resource and user intervention. Instead, at  
84 continental-scale command line interface (CLI) software packages are the best candidates for the  
85 preparation of flood inundation models since they provide robustness and computational efficiency. CLI  
86 packages can also be simpler and more streamlined than general GIS software, providing only the  
87 functionality that users need and thus making sophisticated flood inundation modelling more accessible  
88 to specialist users.

89

90 In this paper we present LFPtools, a Python CLI package which attempts to encompass the most  
91 commonly used methods to prepare input data for flood inundation studies using LISFLOOD-FP  
92 (Sampson et al., 2015; Schumann et al., 2013; Hawker et al., 2018) a widely used flood inundation  
93 model. Among the capabilities LFPtools can provide are: DEM upscaling, bank elevation estimation,  
94 bed elevation estimation, river width subtraction and interpolation, elevation smoothing algorithms,  
95 continent basin splitting, and more. Whilst the software has been built specifically for the LISFLOOD-

96 FP model, many of the operations it encodes are useful for a wide range of other flood inundation  
 97 models, especially those operating on regular grids. LFPtools can act as an intermediate platform to  
 98 streamline the preparation of local, continental or global flood inundation studies in different fields by  
 99 bringing ease of use to non-expert users and efficiency to expert ones. For example, new experimental  
 100 studies on hydrological-hydrodynamic modelling, sensitivity analysis (SAFE Toolbox [Pianosi et al.,](#)  
 101 [2015](#); SALib [Herman et al., 2017](#)) will be achievable more straightforwardly. LFPtools is open-source  
 102 and presents a series of tools to estimate the variables required for flood inundation modelling in rapid  
 103 and automated manner. As open-source, users can revise the code, modify or add new methods easily  
 104 and transparently. The tools were verified over the Severn basin where a 1 km flood inundation model  
 105 was built in under 2 minutes on a standard laptop (1.6 GHz Intel Core i5; 8 GB 1600 MHz DDR3).

## 107 2 The flood model LISFLOOD-FP

108 LISFLOOD-FP ([Bates et al., 2010](#)) is a floodplain inundation model which solves the Saint-Venant  
 109 equations at very low computational cost by neglecting the flow advection term, as this is unimportant  
 110 for typical gradually varying and subcritical floodplain flows. The implementation of LISFLOOD-FP Sub-  
 111 Grid ([Neal et al., 2012](#)) extends the two-dimensional model for application to large domain areas where  
 112 channels may be smaller than typical grid resolutions by treating river and floodplain channel networks  
 113 as sub-grid scale features. Sub-grid topographic information such as realistic river width estimates is  
 114 important since it increases model accuracy in terms of water level simulation, wave propagation speed,  
 115 and inundation extent ([Yamazaki et al., 2011](#); [Neal et al., 2012](#)).

117 Hydrodynamics in LISFLOOD-FP are solved using a momentum equation derived from the quasi-  
 118 linearized one-dimensional form of the Saint-Venant equation described in Eq. (1) where  $q$  is the flow  
 119 per unit width,  $h$  is the flow depth,  $z$  is the bed elevation,  $g$  is the acceleration due to gravity,  $n$  is the  
 120 Manning's friction coefficient and  $R$  is the hydraulic radius which for wide shallow flows can be  
 121 approximated with the flow depth  $h$ .

$$124 \frac{\delta q}{\delta t} + \frac{gh\delta(h+z)}{\delta x} + \frac{gn^2q^2}{R^{4/3}h} = 0 \quad (1)$$

125  
 126 The final form of the unit flow at the next time step is obtained by discretising Eq. (1) with respect to the  
 127 time step  $\Delta t$  as described in Eq. (2):

$$129 q_{t+\Delta t} = \frac{q_t - gh_t\Delta t \frac{\partial(h_t+z)}{\partial x}}{(1 + gh_t\Delta t n^2 q_t / h_t^{10/3})} \quad (2)$$

130  
 131 The model has been widely used for different applications at small and large scales ([Wilson et al., 2007](#);  
 132 [Biancamaria et al., 2009](#); [Neal et al., 2012](#); [Schumann et al., 2013](#); [Schumann et al., 2016](#); [Alfieri et al.,](#)  
 133 [2014](#); [Sampson et al., 2015](#); [Wing et al., 2018](#)) due its computational speed which is mainly given by

134 neglecting the flow advection in the shallow water equation but also by employing a highly efficient finite  
135 difference numerical solution scheme (de Almeida et al., 2012; de Almeida and Bates, 2013).

136

137 The reader is advised to consult the user manual (Bates et al., 2013) for more information on technical  
138 aspects.

139

### 140 **3 Capabilities and features of LFPtools**

141

142 LFPtools is written in Python and built on top of well-known open-source libraries: GDAL, Cython,  
143 Pandas, Numpy and xarray. The TauDEM toolbox (Tarboton, 2005) is also required for some  
144 functionalities. The library handles I/O operations via well-known file formats such as ESRI Shapefiles  
145 and GeoTIFF.

146

#### 147 **3.1 Floodplain elevations**

148

149 Floodplain elevations define the grid output resolution. Those elevations can be obtained directly using  
150 a Digital Elevation Model (DEM) as-is (i.e. at native resolution). Alternatively, if the native DEM contains  
151 noise, usually derived from instrument error, upscaling the native data will reduce that noise in a coarser  
152 floodplain elevation grid, but may also smooth or lose important small scale elevation features (Neal  
153 et al., 2012; Hawker et al., 2018).

154

155 *lfp-rasterresample* is the program included in the library to upscale DEMs. The program can handle  
156 arrays of any size since it never loads entire arrays on memory but instead it loads a small portion  
157 of the array corresponding to the aggregation kernel to be upscaled. The program receives three inputs:  
158 a high-resolution DEM, a target resolution mask and a searching window threshold. Only cells with  
159 mask=1 will be considered for calculation. The upscaling method is described as follows:

160

- 161 1. A user-defined threshold is applied to a centre cell of the target mask to lump together high-resolution  
162 values.
- 163 2. A modified z-score (Iglewicz and Hoaglin, 1993; based on the median absolute deviation) is  
164 calculated for every DEM cell in the kernel. z-score values larger than 3.5 are identified as outliers  
165 and subsequently removed from the aggregation kernel.
- 166 3. In the aggregation kernel, different reduction algorithms can be applied (e.g., mean, min, meanmin).  
167 'meanmin' is an interesting reduction method which averages the minimum and mean values from  
168 the kernel and emphasises topographic valleys in the calculation. Important to mention that more  
169 reduction algorithms can be easily added in the source code by users should they be required.

170

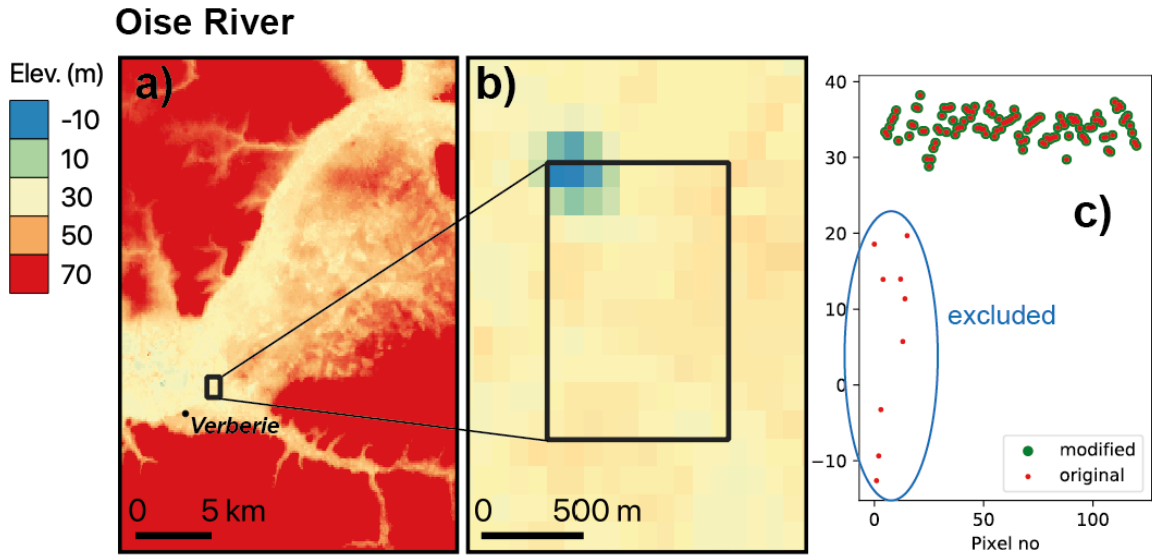
171 Step 2 is important to consider since native DEMs might present irregularities in some places. For  
172 example, in development testing a disagreement was found in the aggregation kernel for a target cell  
173 in the Seine River using the native ~90 m resolution MERIT DEM. In particular, some strong negative

174 values (~-10 m) were found in an area where the typical topographic elevation was ~30 m (See Fig. 1).  
 175 The automatic detection algorithm in step 2 prevents inclusion of these values before step 3.

176

177 Different aggregation methods from Step 3 are compared for a small part of the River Thames using  
 178 the toolbox in Fig. 2.

179

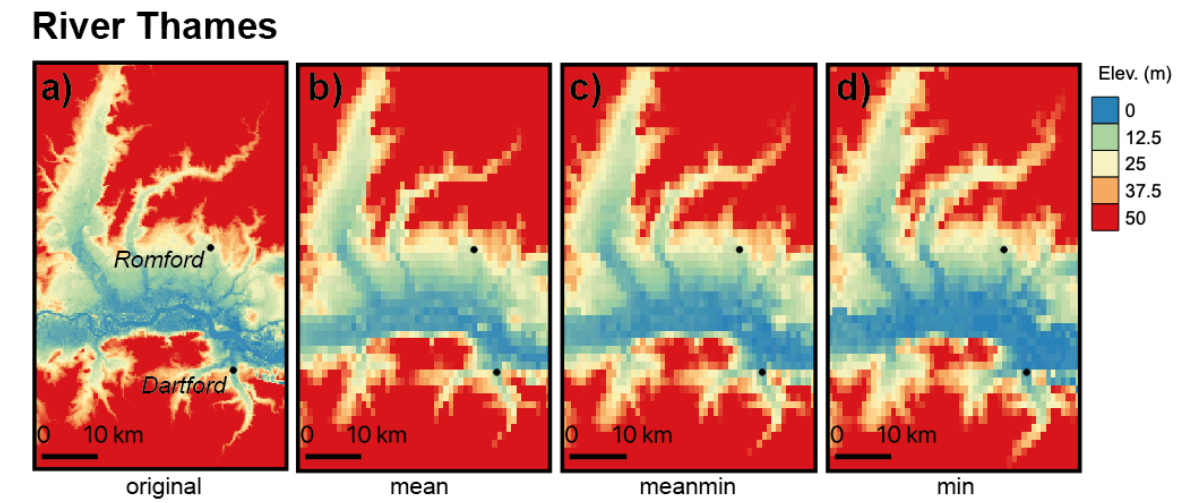


180

181 **Figure 1:** Outlier detection procedure: a) original 90 m resolution DEM and aggregation kernel (in  
 182 black), b) zoom-in at aggregation kernel (area ~1 km<sup>2</sup>) and c) automatic detection of outliers in kernel  
 183 (in green) points retained for upscaling and (in red) all points.

184

185



186

187 **Figure 2:** Upscaling methods comparison at 1 km resolution: a) original 90 m resolution DEM, b)  
 188 'mean' aggregation, c) 'meanmin' aggregation and d) 'min' aggregation

189

190

191 **3.2 Channel widths**

192

193 LISFLOOD-FP Sub-Grid needs several input variables to run a flood simulation, one of which is river  
194 width estimates at every cell in the river network. With the appearance of global river width data sets  
195 based on remote sensing techniques (GWD-LR Yamazaki et al., 2014; GRWL Allen and Pavelsky 2018)  
196 and empirical formulations (Andreadis et al., 2013) it is now feasible to use these data sets as width  
197 sources in flood studies for data-sparse regions.

198

199 Global river width databases may have some degree of geolocation shift in relation to the corresponding  
200 rivers extracted from hydrography databases making them difficult to use in their native format. This  
201 problem may appear if these databases are derived from different sources or due to resolution  
202 dissimilarity; for example, DEM derived river networks and remotely sensed open water locations.  
203 Commonly, a nearest neighbour function in a searching window is used to assign the nearest value  
204 from a river width database to a river cell in a flood study. However, there might be cases where the  
205 searching window is too small and no width values are found, in this case increasing the window size  
206 is not an appealing option since it might result in an incorrect river width assignment from a tributary.  
207 Instead, it is advisable to use an interpolation with values already assigned. It is important to note that  
208 leaving a river cell with no width assigned is a critical issue since LISFLOOD-FP Sub-Grid cannot  
209 perform calculations on river cells with zero width.

210

211 LFPtools includes a routine (*lfp-getwidths*) to automatically assign width values to river cells, it works in  
212 the following way:

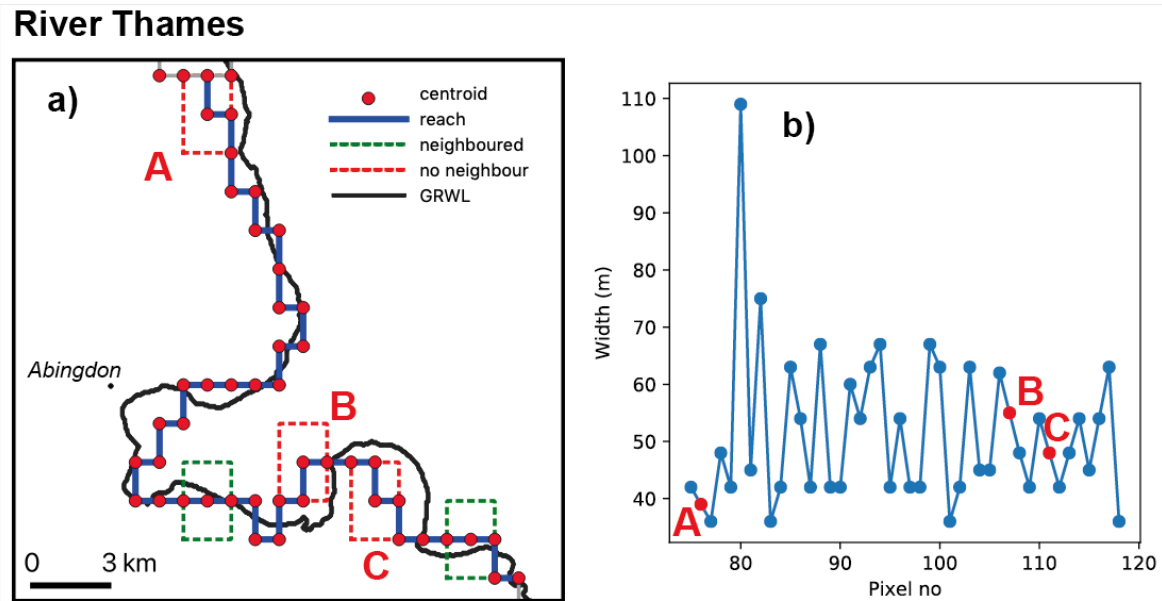
213

- 214 1. River cell widths are assigned based on the nearest-neighbour within a searching window.
- 215 2. If no width value is assigned from the source database, the missing value is automatically  
216 interpolated with values already assigned.

217

218 Fig. 3 shows an example of three river cells with widths unassigned due to the searching window size  
219 problem. Fig. 3a shows a river reach (blue) at ~1 km, red dots are centroids of river cells and the black  
220 solid line is river vector from the GRWL database (~30 m). From the figure only three points (A, B, C)  
221 were not able to find an appropriate width value in their neighbourhood (red dash line), those values  
222 were automatically calculated by interpolation in *lfp-getwidths* see Fig. 3b

223



224

225 **Figure 3:** River widths assignment: **a)** Example showing three river cells unassigned due to small size  
 226 in searching window at locations A, B and C and **b)** (in blue) width values that yield in the searching  
 227 window (in red) width values interpolated.

228

229

230

### 231 3.3 Bank elevations

232

233 The LISFLOOD-FP Sub-Grid uses the DEM elevation as the bank height elevations, which when  
 234 combined with the channel bed elevation defines the channel bankfull depth. It is therefore  
 235 recommended to recalculate the bank height elevations to get better estimates because of the critical  
 236 role this value plays in flooding simulations.

237

238 If a native resolution DEM is used, bank height elevations are self-defined. However, if a coarser  
 239 resolution model is created, high-resolution cell aggregation is required. *lfp-getbankelevs* reads a target  
 240 river network mask (mask=1 will be considered for calculation), a high-resolution DEM, and a searching  
 241 window threshold to aggregate cells and apply a reduction algorithm (nearest, mean, min, meanmin).  
 242 Resulting elevations might contain irregularities that may result in model instabilities caused by local  
 243 supercritical flows and flow blocking effects if the channel bed follows the banks. Those irregularities  
 244 can be solved by applying a smoothing algorithm along the river.

245

246 LFPtools includes a routine (*lfp-fixelevs*) which includes two approaches to deal with this problem:

247

248 1. Adjust bank heights by minimising the amount of modifications following the method developed by  
 249 [Yamazaki et al., \(2012\)](#). This algorithm removes all the pits in the spaceborne DEM caused by



250 vegetation canopies, sub-pixel sized structures, and random radar speckles while minimizing the  
 251 amount of modification required for removing the pits.

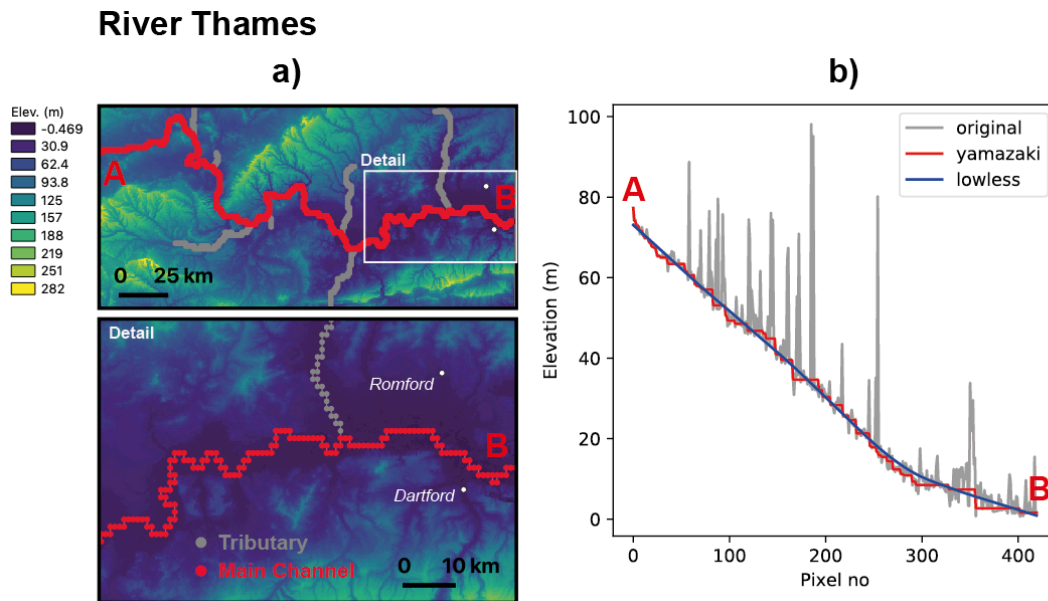
252 2. Apply a weighted local regression (LOWLESS) (Cleveland, 1979) in the downstream direction as in  
 253 [Schumann et al., \(2013\)](#).

254

255 Both methods are compared for the main channel of the River Thames, UK in Fig. 4b

256

257



258

259 **Figure 4:** Smoothing method available in LFPtools. These methods were applied to the main channel  
 260 of the River Thames: **a)** (in red) main channel of the River Thames and (in grey) tributaries, **b)** (in  
 261 grey) original elevation extracted by the nearest-neighbour (in red) Yamazaki's method (in blue)

262 Locally weighted smoothing

263

264

265

### 266 3.4 River depths

267

268 Standard LISFLOOD-FP Sub-Grid treats river cross-sections as rectangular. Due to this fact channel  
 269 depths may differ from in-situ river depth surveys. With some calibration this approximation works very  
 270 well at large scales producing reasonable results in most places as long as accurate estimations of  
 271 bank heights and widths are used. Unlike bank heights and river widths that can be determined from  
 272 satellite data, river depths need to be approximated. Two approaches have been proposed to achieve  
 273 this goal and are included in the *lfp-getdepths* tool — a simple empirical power law formulation ([Neal et](#)  
 274 [al., 2012](#)) and the Manning's equation ([Sampson et al., 2015](#)). A user-defined raster (e.g., survey data  
 275 on river bathymetry) can also be used to assign depths to cells if none of the previous methods are  
 276 used.

277

278 **Power law relationship**

279

280 [Leopold and Maddock \(1953\)](#) derived a series of power law relationships given by Eq. (5), (6) and (7)281 where  $W$  is water-surface width,  $Q$  is discharge,  $D$  is mean depth and  $V$  is mean velocity

282

283 
$$W = aQ^b \quad (3)$$

284 
$$D = cQ^f \quad (4)$$

285 
$$V = kQ^m \quad (5)$$

286

287 It is straightforward to equate Eq. (3) and (4) to obtain Eq. (6)

288

289 
$$D = \left(\frac{c}{af/b}\right) W^{f/b} \quad (6)$$

290

291 where  $(a, b, c, f)$  are empirical values depending on the geomorphology of the bed. Sometimes it is  
 292 preferred to use only one pair of constants  $(r, p)$  as in Eq. (7). See [Hey and Thorne \(1986\)](#) for empirical  
 293 values for gravel-bed rivers in the UK.

294

295 
$$D = rW^p \quad (7)$$

296

297

298 **Manning's equation**

299

300 The Manning's equation for a rectangular channel is described by Eq. (8) where  $A$  is the cross-section  
 301 area expressed as  $A = WD$  with  $W$  width and  $D$  depth,  $R$  is the hydraulic radius  $R = A/(W + 2D)$ ,  $S$  is  
 302 the channel cell slope—it can be calculated via *lfp-slopes* or directly extracted from an external data  
 303 set ([Cohen et al., 2018](#))— $n$  is the Manning's coefficient and  $Q_{bf}$  is the bankfull flow.

304

305 
$$Q_{bf} = \frac{AR^{2/3}S^{1/2}}{n} \quad (8)$$

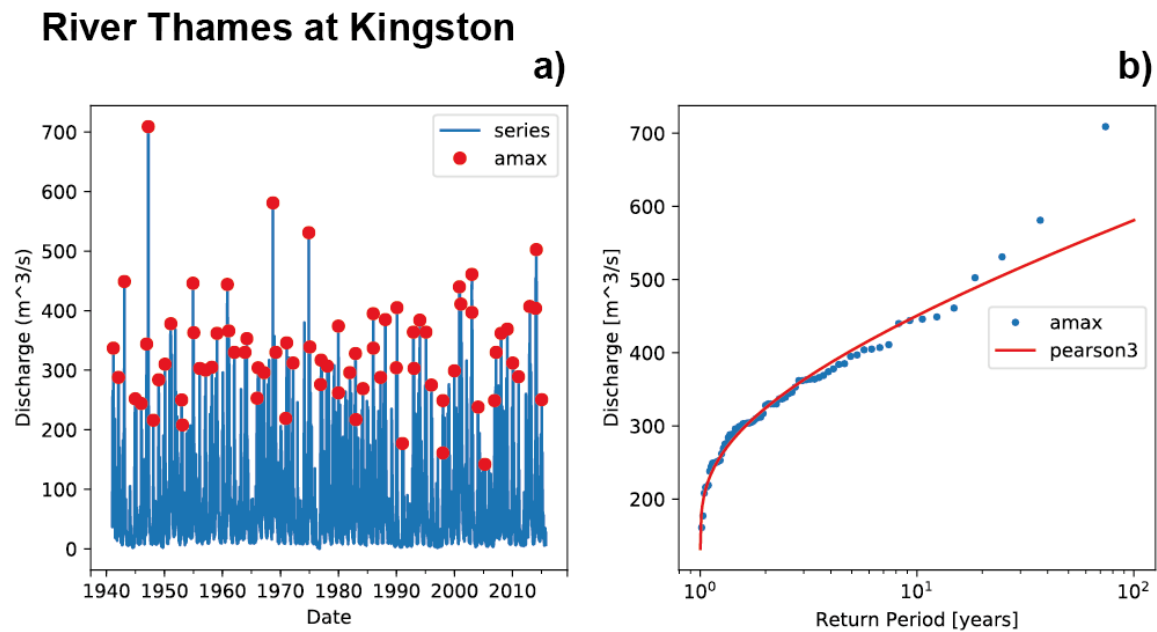
306

307 The Manning's equation considers bankfull flow  $Q_{bf}$  as a known variable, however it is not always the  
 308 case. If not measured in the field, bankfull flow is usually estimated by fitting a statistical distribution on  
 309 the annual flow peaks of a streamflow time series where bankfull conditions occur at return periods of  
 310 1.5-2 years ([Schneider et al., 2011](#)). Fig. 5 shows the aforementioned procedure for the Kingston  
 311 gauging station from the National River Flow Archive (NRFA) on the River Thames, UK.

312

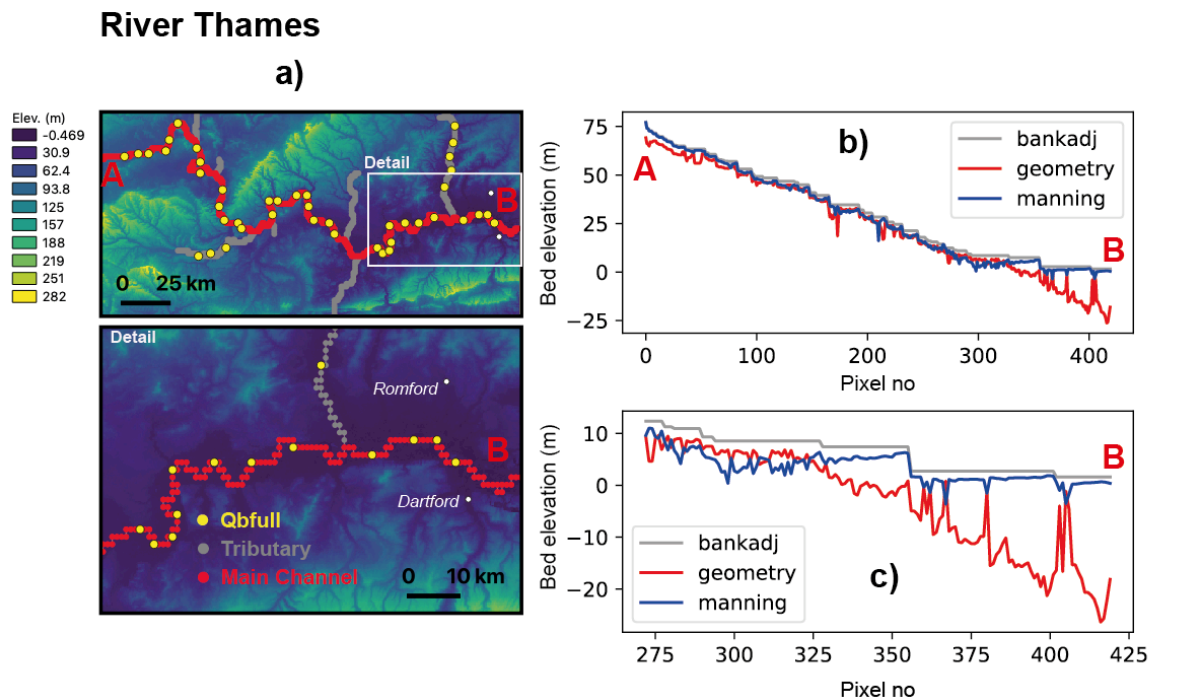
313 A comparison between the Power law relationship and Manning's equation is presented for the River  
 314 Thames in Fig. 6. Bankfull flow (yellow dots) was obtained by subtracting the 2-year return period in a  
 315 Pearson Type III distribution fitted on the annual maxima time series derived by means of a 24-year

316 streamflow reanalysis from the European Forecasting Awareness System (EFAS) (Thielen et al., 2009).  
 317 River width estimates used in Eq. (7) were obtained from the GRWL database using *lfp-getwidths*. At  
 318 locations where no-bankfull width is available, the nearest bankfull value was assigned. Fig 6c shows  
 319 (in grey) bank elevations after smoothing in the main channel, (in blue) bed elevations (i.e., bank  
 320 elevation - depth) using the Manning's Eq. (8) and (in red) using the power law relationship Eq. (7). A  
 321 zoom for the downstream section is shown in Fig 6d and reveals considerable differences in the delta  
 322 area.  
 323  
 324



325  
 326 **Figure 5:** Observed river discharge in the River Thames at Kingston Station. Bankfull was estimated  
 327 by fitting a statistical distribution on the annual maxima and retrieving the discharge value for the 2-yr  
 328 return period: **a)** annual maxima between 1940-2015 (red dots). **b)** Pearson Type III distribution fitted  
 329 on the annual maxima (red line), here the distribution parameters were estimated via L-moments. This  
 330 figure was generated by using the *hydrouils* library (Sosa, 2018).

331



332

333

334

335

336

337

338

339

340

341

342

343

344

### 3.5 Continental tools

345

346

347

348

349

350

351

352

353

354

355

356

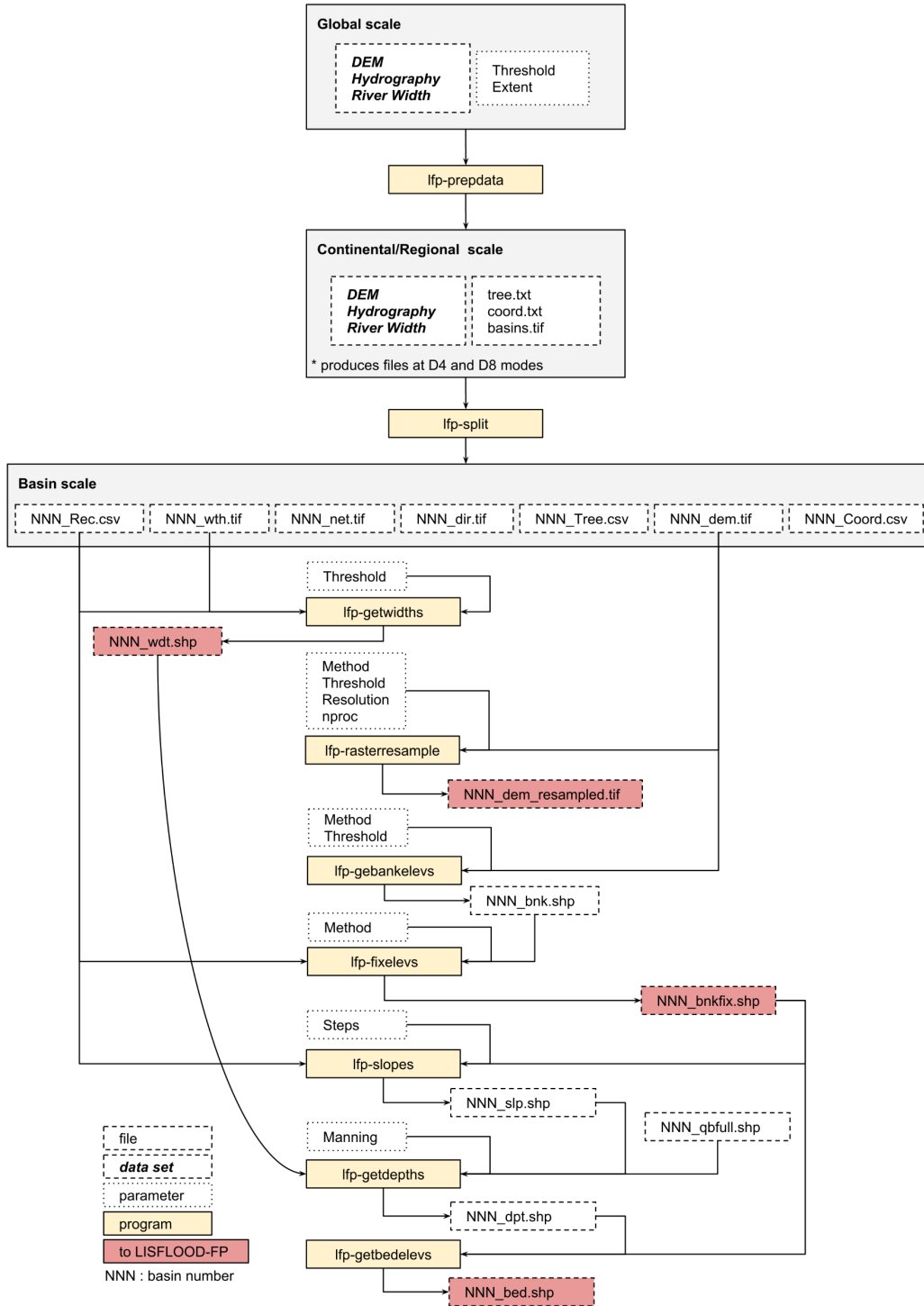
**Figure 6:** River depth estimation using hydraulic geometry equations and Manning's equation: **a)** River Thames (in red) tributaries (in grey), **b)** depth estimation via hydraulic geometry (in red) and Manning's equation (in blue) for the lower part of the River Thames and **c)** zoom-in delta area of the River Thames

The library includes two programs designed to automate delineation of basins within large regions *lfp-prepdata* and *lfp-split*.

*lfp-prepdata* incorporates a subroutine to clip global data sets of DEM, hydrography and river width based on a user-defined extent. Thereafter, a user-defined threshold is applied to the flow accumulation area (or upslope drainage area) to define a river network. The TauDEM toolbox (Tarboton, 2005) is used to generate a network topological connectivity for the whole area and to delineate basins within the region (NNN\_Tree.csv, NNN\_Coord.csv and NNN\_Rec.csv in Fig. 7). The routine also includes a function to convert D8 connected river networks to D4 connectivity based on the flow directions map given by the hydrography. *lfp-split* breaks up the region into individual basins with a basin-number associated. Folders are created with a basin-number and each of them contains clipped data associated

357 with that basin. After basin required data is split in this way the tools described in Sections 3.1-3.4 can  
 358 be applied. Fig. 7 shows a flowchart describing how the tools can connect to each other to automatically  
 359 build models at continental-scale.

**LFPtools flowchart**



360  
 361

362 **Figure 7:** Flowchart using LFPtools for continental-scale studies. Command-line tools are presented  
 363 in yellow boxes, white dashed boxes represent input data sets and white dotted boxes free  
 364 parameters. Outputs to LISFLOOD-FP are coloured in red.

365

### 366 3.6 Usage

367

368 In order to facilitate the use of the tools LFPtools can be called via command-line, however if preferred  
 369 it can also be imported as a Python module. All tools can be invoked via the command line by typing  
 370 the name of the tool followed by the `-i` keyword and the name of the configuration file:

371

```
372 $ lfp-getwidths -i config.txt
```

373

374 where the configuration file 'config.txt' is a text file containing a [tool-name] header followed by  
 375 variable=argument entries. Input variable descriptions are specified when typing the name of the tool  
 376 in the command-line followed by the `-h` keyword: `$ lfp-getwidths -h`

377

378 LFPtools can be imported as a Python module as follows:

379

```
380 import lfp as lfp
```

381

382 An overview of tools with a brief description is given in Table 1.

383

384

Program	Description
lfp-depths	Get estimates of depth
lfp-fixelevs	Smooth elevations
lfp-getbankelevs	Retrieve bank elevations
lfp-slopes	Estimate slopes in a river network
lfp-getwidths	Retrieve river widths
lfp-rasterresample	Upscale a high-resolution DEM into a user-defined resolution
lfp-split	Breaks up a study area in individual basins with a basin number associated
lfp-prepdata	Clip global data sets given a user-defined extent and threshold. The threshold is used to define a river network based on the upslope area

385

386

**Table 1:** Summary of programs in LFPtools

387

388

389  
 390  
 391  
 392  
 393  
 394  
 395  
 396  
 397  
 398  
 399  
 400  
 401  
 402  
 403  
 404  
 405  
 406  
 407

#### 4 A flood inundation model for the Severn River in England, UK

LFPTools was used to build a flood inundation model for the Severn river basin in the UK. A one-month simulation (April 1998) was undertaken in order to capture an observed flood event that happened during this period. An additional one month 'warm-up' period was included to bring the model into a hydraulic steady state condition prior to the commencement of the April 1998 period. The model was built from LIDAR-based terrain data (at 90 m resolution) where the floodplain terrain was upscaled to 1 km resolution using the 'mean' aggregation method and removing outliers. Bank heights were defined using the 'nearest neighbour' method. River channels were explicitly represented using HydroSHEDS (Lehner et al., 2008) as input hydrography at 1 km resolution. Channel widths were retrieved from the GRWL database while river depths were estimated through the hydraulic geometry method (Eq. 5) with  $r = 0.12$  and  $p = 0.78$ . The model was forced using daily gauged flows from the UK National River Flow Archive (NRFA) for the simulation period mentioned before. Data sources used in this study are briefly described in Table 2.

Data set	Description	Source
LIDAR DTM	Composite at 1 m resolution	Data available at data.gov.uk
HydroSHEDS	Hydrography at 1 km resolution	Lehner et al., 2018. Data available at hydrosheds.org
GRWL	Landsat-based global river width database at 30 m resolution	Allen and Pavelsky, 2018. Data available at <a href="https://zenodo.org/record/1297434">https://zenodo.org/record/1297434</a>
NRFA	Streamflow data from gauge stations	Data available at nrfa.ceh.ac.uk
Recorded Flood Outlines for UK	Records of historic flooding from rivers, the sea, groundwater and surface water	Data available at data.gov.uk

408  
 409  
 410  
 411  
 412  
 413  
 414  
 415  
 416

**Table 2:** Data sets used to build the flood inundation model in the Severn river basin

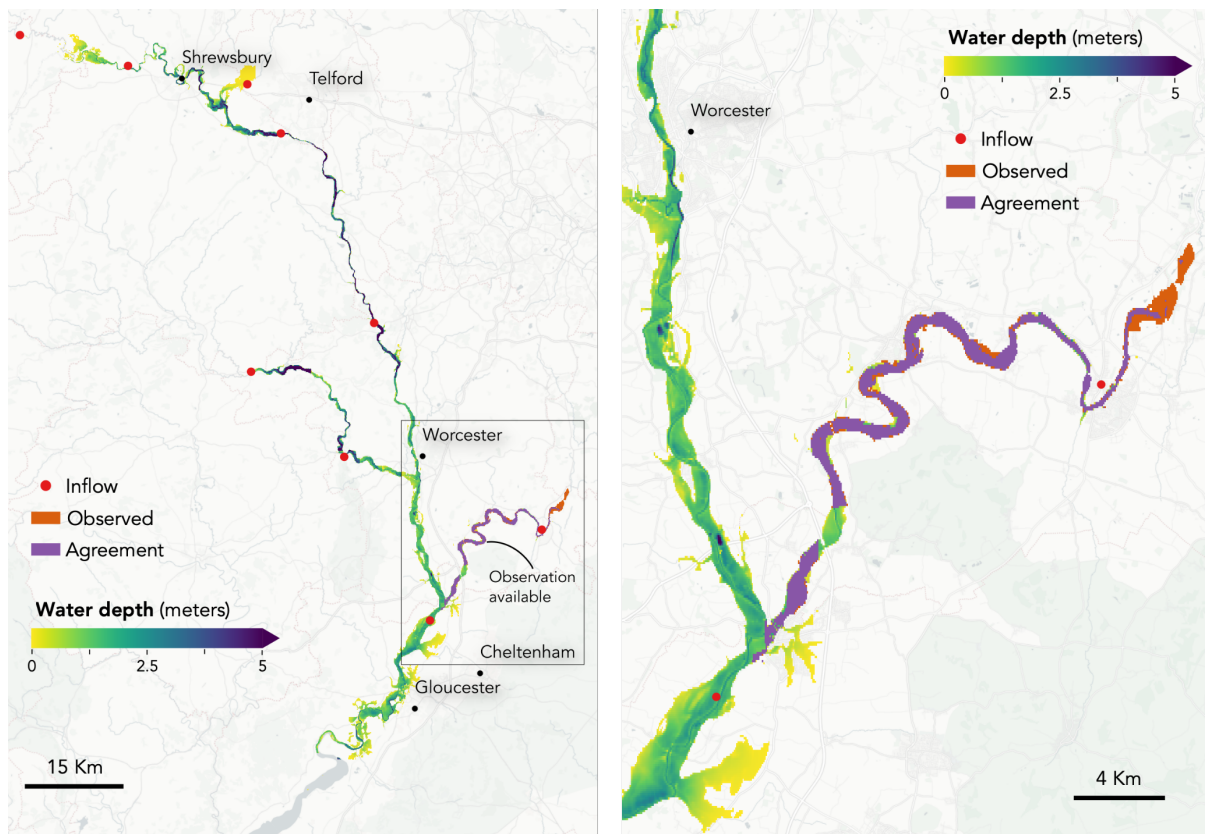
Resulting water depths from LISFLOOD-FP at 1 km resolution were subsequently downscaled onto 90 m resolution using an algorithm similar to Schumann et al., 2014. In particular, the algorithm takes water surface elevation (WSE) at 1 km resolution and subtracts its corresponding 90 m DEM values. From this arithmetic operation, a grid at 90 m resolution is created with positive values representing the water depth (wet cells) whilst negative values (dry cells) are replaced with nodata values.

417 The performance of flood model in the Severn river basin in terms of flood extent was quantified using  
 418 three scores: Hit rate (H), Falsa alarm ratio (F) and Critical success index (C). *H* tests the tendency of  
 419 the model towards underprediction and can range from 0 (none of the wet benchmark data is wet model  
 420 data) to 1 (all of the wet benchmark data are wet model data). *F* examines the tendency of the model  
 421 towards overprediction and can range from 0 (no false alarms) to 1 (all false alarms). *C* accounts for  
 422 both overprediction and underprediction and can range from 0 (no match between modelled and  
 423 benchmark data) to 1 (perfect match between modelled and benchmark data). A detailed explanation  
 424 of these scores is available in Wing et al., 2017.

425

426 Simulated water depth results for the 15<sup>th</sup> April 1998 are shown in Fig. 8. From the figure is clear that  
 427 in most places water remains in the channel and where water elevations exceed bankfull heights water  
 428 spreads onto the floodplains. Simulated water depth on the 15<sup>th</sup> April 1998 were compared with the  
 429 official event footprint from the English Environment Agency (EA) and the 'Agreement' between both  
 430 flood extents are presented in the Fig. 8 right-hand panel. The 'Agreement' in Fig. 8 refers to areas in  
 431 the map where the EA flood extent and the simulated flood extent overlap each other. In terms of flood  
 432 extent, the model obtained satisfactory comparison scores against observations:  $H=0.79$ ,  $F=0.24$  and  
 433  $C=0.63$ . Example files are available at the LFPtools web repository.

434



435

436 **Figure 8:** Flood inundation model prepared for the Severn basin in England, UK during the flood  
 437 event of April-1998. The event was compared with official footprint of the event (orange). The  
 438 agreement between the model and the output is also shown (purple). Note that the observed data  
 439 only cover limited portions of the model domain which are not contiguous. In areas with no observed



440 data we simply plot the modelled water depth. Also, the moderately low *Hit Rates* occur since the  
441 observed flood extent area is upstream of the inflow point (East of the domain in the right-hand  
442 panel), hence, no forcing data is available to predict water depths in that area.

443

444

445

## 446 **5 Conclusions**

447

448 A Python CLI package has been developed to help prepare input data for flood studies carried out using  
449 LISFLOOD-FP. The package encompasses the most frequently used methods for flood inundation  
450 modelling data preparation, and also facilitates the addition of new ones if desired. LFPtools can be  
451 thought of as a platform to streamline the preparation of flood inundation studies in different fields by  
452 bringing ease of use to non-expert users and efficiency to expert ones. It is built on top of the state-of-  
453 the-art Python libraries to handle large sets of data and it is in active development. It is important to  
454 mention that these tasks could be done in a GIS package, but only with quite extreme difficulty and for  
455 small data arrays. The tasks performed by LFPTools are generic for structured grids and can be used  
456 to prepare input data sets for any hydraulic model.

457

458 LFPtools programs were verified in the UK's Severn basin on a model built at 1 km resolution using  
459 publicly available data sets only. The test basin was used to simulate the event of April 1998 and results  
460 are presented in Fig. 8. From the figure it is clear that most of the water is kept in channels with some  
461 places inundated suggesting a normal hydrodynamic behaviour. After comparison, the model obtained  
462 satisfactory scores against the official event footprint:  $H=0.79$ ,  $F=0.24$  and  $C=0.63$ . It is important to  
463 mention that the Severn scenario was used only to broadly test the tools and not to simulate the real  
464 event to an engineering standard.

465

466 The Severn river basin used in this study is only a small example on how the tools can be employed  
467 and the tools have been designed so they can be integrated within a framework to build continental to  
468 global scale studies. For example, LFPtools can be used within a modelling framework to build a  
469 continental-scale flood hindcast or reanalysis, a modelling framework of continental-scale flood extent  
470 for an early warning system or even within a framework to predict flood inundation variables (flood  
471 extent, water depth, etc) in a climate change context.

472

473 Global to continental scale models are being used by insurers, multi-national corporations, NGOs and  
474 national governments to tackle problems such as rapid flood disaster response, urban planning and  
475 climate change adaptation. Thus, flood models at such scales are important decision making tools and  
476 building them demands great effort to research scientists. We envisage that this innovative set of tools  
477 will help to significantly reduce these costs.

478

479

**480 Acknowledgments**

481 J.S. received funding from the European Union's Horizon 2020 research and innovation programme  
482 under the Marie Skłodowska-Curie grant agreement No. 676027. P.B. was supported by a Leverhulme  
483 Research Fellowship and a Wolfson Research Merit Award from the Royal Society. The  
484 authors would like to thank Gemma Coxon for providing the NRFA data.

485

**486 References**

487

488 Alfieri, L., Dottori, F., Betts, R., Salamon, P., Feyen, L., 2018. Multi-Model Projections of River Flood  
489 Risk in Europe under Global Warming. *Climate* 6, 6. <https://doi.org/10.3390/cli6010006>

490

491 Alfieri, L., Salamon, P., Bianchi, A., Neal, J., Bates, P., Feyen, L., 2014. Advances in pan-European  
492 flood hazard mapping. *Hydrol Process* 28, 4067–4077. <https://doi.org/10.1002/hyp.9947>

493

494 Allen, G.H., Pavelsky, T.M., 2018. Global extent of rivers and streams. *Science*.

495 <https://doi.org/10.1126/science.aat0636>

496

497 Andreadis, K.M., Schumann, G.J.-P., Pavelsky, T., 2013. A simple global river bankfull width and  
498 depth database: Data and Analysis Note. *Water Resour Res* 49, 7164–7168.

499 <https://doi.org/10.1002/wrcr.20440>

500

501 Bates, P., Trigg, M., Neal, J., Dabrowa, A., 2013. LISFLOOD-FP user manual. School of  
502 Geographical Sciences, University of Bristol, UK.

503

504 Bates, P.D., Horritt, M.S., Fewtrell, T.J., 2010. A simple inertial formulation of the shallow water  
505 equations for efficient two-dimensional flood inundation modelling. *J Hydrol* 387, 33–45.

506 <https://doi.org/10.1016/j.jhydrol.2010.03.027>

507

508 Biancamaria, S., Bates, P.D., Boone, A., Mognard, N.M., 2009. Large-scale coupled hydrologic and  
509 hydraulic modelling of the Ob river in Siberia. *J Hydrol* 379, 136–150.

510 <https://doi.org/10.1016/j.jhydrol.2009.09.054>

511

512 Bradbrook, K.F., Lane, S.N., Waller, S.G., Bates, P.D., 2004. Two dimensional diffusion wave  
513 modelling of flood inundation using a simplified channel representation. *Intl. J. River Basin*

514 *Management* 2, 211–223. <https://doi.org/10.1080/15715124.2004.9635233>

515

516 Cleveland, W.S., 1979. Robust Locally Weighted Regression and Smoothing Scatterplots. *Journal of*  
517 *the American Statistical Association* 74, 829–836. <https://doi.org/10.1080/01621459.1979.10481038>

518

- 519 Cohen, S., Wan, T., Islam, M.T., Syvitski, J.P.M., 2018. Global river slope: A new geospatial dataset  
 520 and global-scale analysis. *J Hydrol* 563, 1057–1067. <https://doi.org/10.1016/j.jhydrol.2018.06.066>  
 521
- 522 de Almeida, G.A.M., Bates, P., 2013. Applicability of the local inertial approximation of the shallow  
 523 water equations to flood modeling. *Water Resour Res* 49, 4833–4844.  
 524 <https://doi.org/10.1002/wrcr.20366>  
 525
- 526 de Almeida, G.A.M., Bates, P., Freer, J.E., Souvignet, M., 2012. Improving the stability of a simple  
 527 formulation of the shallow water equations for 2-D flood modeling. *Water Resour Res* 48.  
 528 <https://doi.org/10.1029/2011WR011570>  
 529
- 530 Dottori, F., Kalas, M., Salamon, P., Bianchi, A., Alfieri, L., Feyen, L., 2017. An operational procedure  
 531 for rapid flood risk assessment in Europe. *Nat Hazards Earth Syst Sci* 17, 1111–1126.  
 532 <https://doi.org/10.5194/nhess-17-1111-2017>  
 533
- 534 Farr, T.G., Rosen, P.A., Caro, E., Crippen, R., Duren, R., Hensley, S., Kobrick, M., Paller, M.,  
 535 Rodriguez, E., Roth, L., Seal, D., Shaffer, S., Shimada, J., Umland, J., Werner, M., Oskin, M.,  
 536 Burbank, D., Alsdorf, D., 2007. The Shuttle Radar Topography Mission. *Rev Geophys* 45.  
 537 <https://doi.org/10.1029/2005RG000183>  
 538
- 539 Hawker, L., Rougier, J., Neal, J., Bates, P., Archer, L., Yamazaki, D., 2018. Implications of Simulating  
 540 Global Digital Elevation Models for Flood Inundation Studies. *Water Resour Res* 54, 7910–7928.  
 541 <https://doi.org/10.1029/2018WR023279>  
 542
- 543 Herman, J., Usher, W., 2017. SALib: An open-source Python library for Sensitivity Analysis. *The*  
 544 *Journal of Open Source Software* 2, 97. <https://doi.org/10.21105/joss.00097>  
 545
- 546 Hey, R.D., Thorne, C.R., 1986. Stable Channels with Mobile Gravel Beds. *J Hydraul Eng* 112, 671–  
 547 689. [https://doi.org/10.1061/\(ASCE\)0733-9429\(1986\)112:8\(671\)](https://doi.org/10.1061/(ASCE)0733-9429(1986)112:8(671))  
 548
- 549 Iglewicz, B. and Hoaglin, D.C., 1993. How to detect and handle outliers (Vol. 16). Asq Press.  
 550
- 551 Lamb, R., Crossley, M., Waller, S., 2009. A fast two-dimensional floodplain inundation model.  
 552 *Proceedings of the Institution of Civil Engineers - Water Management* 162, 363–370.  
 553 <https://doi.org/10.1680/wama.2009.162.6.363>  
 554
- 555 Lehner, B., Verdin, K., Jarvis, A., 2008. New Global Hydrography Derived From Spaceborne  
 556 Elevation Data. *Eos, Transactions American Geophysical Union* 89, 93.  
 557 <https://doi.org/10.1029/2008EO100001>  
 558

- 559 Leopold, L.B., Maddock Jr., T., 1953. The hydraulic geometry of stream channels and some  
560 physiographic implications (Report No. 252), Professional Paper. Washington, D.C.  
561
- 562 Lu, X., Zhuang, Q., Liu, Y., Zhou, Y., Aghakouchak, A., 2016. A large-scale methane model by  
563 incorporating the surface water transport: Development of a Methane Model. *J Geophys Res*  
564 *Biogeosci* 121, 1657–1674. <https://doi.org/10.1002/2016JG003321>  
565
- 566 Neal, J., Dunne, T., Sampson, C., Smith, A., Bates, P., 2018. Optimisation of the two-dimensional  
567 hydraulic model LISFOOD-FP for CPU architecture. *Environ Model Softw* 107, 148–157.  
568 <https://doi.org/10.1016/j.envsoft.2018.05.011>  
569
- 570 Neal, J., Schumann, G., Bates, P., 2012. A subgrid channel model for simulating river hydraulics and  
571 floodplain inundation over large and data sparse areas. *Water Resour Res* 48.  
572 <https://doi.org/10.1029/2012WR012514>  
573
- 574 Pianosi, F., Sarrazin, F., Wagener, T., 2015. A Matlab toolbox for Global Sensitivity Analysis. *Environ*  
575 *Model Softw* 70, 80–85. <https://doi.org/10.1016/j.envsoft.2015.04.009>  
576
- 577 Rizzoli, P., Martone, M., Gonzalez, C., Wecklich, C., Borla Tridon, D., Bräutigam, B., Bachmann, M.,  
578 Schulze, D., Fritz, T., Huber, M., Wessel, B., Krieger, G., Zink, M., Moreira, A., 2017. Generation and  
579 performance assessment of the global TanDEM-X digital elevation model. *Isprs J Photogramm* 132,  
580 119–139. <https://doi.org/10.1016/j.isprsjprs.2017.08.008>  
581
- 582 Sampson, C.C., Smith, A.M., Bates, P.D., Neal, J.C., Alfieri, L., Freer, J.E., 2015. A high-resolution  
583 global flood hazard model. *Water Resour Res* 51, 7358–7381.  
584 <https://doi.org/10.1002/2015WR016954>  
585
- 586 Sanders, B.F., Schubert, J.E., Detwiler, R.L., 2010. ParBreZo: A parallel, unstructured grid, Godunov-  
587 type, shallow-water code for high-resolution flood inundation modeling at the regional scale. *Adv*  
588 *Water Resour* 33, 1456–1467. <https://doi.org/10.1016/j.advwatres.2010.07.007>  
589
- 590 Schneider, C., Flörke, M., Eisner, S., Voss, F., 2011. Large scale modelling of bankfull flow: An  
591 example for Europe. *J Hydrol* 408, 235–245. <https://doi.org/10.1016/j.jhydrol.2011.08.004>  
592
- 593 Schumann, G.J.-P., Andreadis, K.M., Bates, P.D., 2014. Downscaling coarse grid hydrodynamic  
594 model simulations over large domains. *J Hydrol* 508, 289–298.  
595 <https://doi.org/10.1016/j.jhydrol.2013.08.051>  
596

- 597 Schumann, G.J.-P., Neal, J.C., Voisin, N., Andreadis, K.M., Pappenberger, F., Phanthuwongpakdee,  
598 N., Hall, A.C., Bates, P.D., 2013. A first large-scale flood inundation forecasting model: Large-Scale  
599 Flood Inundation Forecasting. *Water Resour Res* 49, 6248–6257. <https://doi.org/10.1002/wrcr.20521>  
600
- 601 Schumann, G.J.-P., Stampoulis, D., Smith, A.M., Sampson, C.C., Andreadis, K.M., Neal, J.C., Bates,  
602 P.D., 2016. Rethinking flood hazard at the global scale. *Geophys Res Lett* 43, 10,249-10,256.  
603 <https://doi.org/10.1002/2016GL070260>  
604
- 605 Sosa, J., 2018. Hydroutils. <https://doi.org/10.5281/zenodo.1408076>  
606
- 607 Syme, W.J., 1991. Dynamically Linked Two-dimensional/One-dimensional Hydrodynamic Modelling  
608 Program for Rivers, Estuaries & Coastal Waters (MEngSc thesis). University of Queensland,  
609 Australia.  
610
- 611 Tadono, T., Takaku, J., Tsutsui, K., Oda, F., Nagai, H., 2015. Status of “ALOS World 3D (AW3D)”  
612 global DSM generation. *Proceeding 2015 IEEE International Geoscience and Remote Sensing*  
613 *Symposium (IGARSS)*, pp. 3822–3825. <https://doi.org/10.1109/IGARSS.2015.7326657>  
614
- 615 Tarboton, D.G., 2005. Terrain analysis using digital elevation models (TauDEM).  
616
- 617 Thielen, J., Bartholmes, J., Ramos, M.-H., de Roo, A., 2009. The European Flood Alert System – Part  
618 1: Concept and development. *Hydrol Earth Syst Sci* 13, 125–140. [https://doi.org/10.5194/hess-13-](https://doi.org/10.5194/hess-13-125-2009)  
619 [125-2009](https://doi.org/10.5194/hess-13-125-2009)  
620
- 621 Villanueva, I., Wright, N.G., 2006. Linking Riemann and storage cell models for flood prediction.  
622 *Proceedings of the Institution of Civil Engineers - Water Management* 159, 27–33.  
623 <https://doi.org/10.1680/wama.2006.159.1.27>  
624
- 625 Wessel, B., Huber, M., Wohlfart, C., Marschalk, U., Kosmann, D., Roth, A., 2018. Accuracy  
626 assessment of the global TanDEM-X Digital Elevation Model with GPS data. *Isprs J Photogramm*  
627 *139*, 171–182. <https://doi.org/10.1016/j.isprsjprs.2018.02.017>  
628
- 629 Wilson, M., Bates, P., Alsdorf, D., Forsberg, B., Horritt, M., Melack, J., Frappart, F., Famiglietti, J.,  
630 2007. Modeling large-scale inundation of Amazonian seasonally flooded wetlands. *Geophys Res Lett*  
631 *34*. <https://doi.org/10.1029/2007GL030156>  
632
- 633 Wing, O.E.J., Bates, P.D., Sampson, C.C., Smith, A.M., Johnson, K.A., Erickson, T.A., 2017.  
634 Validation of a 30 m resolution flood hazard model of the conterminous United States. *Water Resour*  
635 *Res* 53, 7968–7986. <https://doi.org/10.1002/2017WR020917>  
636

637 Wing, O.E.J., Bates, P.D., Smith, A.M., Sampson, C.C., Johnson, K.A., Fargione, J., Morefield, P.,  
638 2018. Estimates of present and future flood risk in the conterminous United States. *Environ Res Lett*  
639 13, 034023. <https://doi.org/10.1088/1748-9326/aaac65>  
640  
641 Winsemius, H.C., Van Beek, L.P.H., Jongman, B., Ward, P.J., Bouwman, A., 2013. A framework for  
642 global river flood risk assessments. *Hydrol Earth Syst Sci* 17, 1871–1892.  
643 <https://doi.org/10.5194/hess-17-1871-2013>  
644  
645 Yamazaki, D., Ikeshima, D., Tawatari, R., Yamaguchi, T., O’Loughlin, F., Neal, J.C., Sampson, C.C.,  
646 Kanae, S., Bates, P.D., 2017. A high-accuracy map of global terrain elevations. *Geophys Res Lett* 44,  
647 5844–5853. <https://doi.org/10.1002/2017GL072874>  
648  
649 Yamazaki, D., Kanae, S., Kim, H., Oki, T., 2011. A physically based description of floodplain  
650 inundation dynamics in a global river routing model. *Water Resour Res* 47.  
651 <https://doi.org/10.1029/2010WR009726>  
652  
653 Yamazaki, D., Baugh, C.A., Bates, P.D., Kanae, S., Alsdorf, D.E., Oki, T., 2012. Adjustment of a  
654 spaceborne DEM for use in floodplain hydrodynamic modeling. *J Hydrol* 436–437, 81–91.  
655 <https://doi.org/10.1016/j.jhydrol.2012.02.045>  
656  
657 Yamazaki, D., O’Loughlin, F., Trigg, M.A., Miller, Z.F., Pavelsky, T.M., Bates, P.D., 2014.  
658 Development of the Global Width Database for Large Rivers. *Water Resour Res* 50, 3467–3480.  
659 <https://doi.org/10.1002/2013WR014664>  
660  
661 Yamazaki, D., Ikeshima, D., Sosa, J., Bates, P.D., Allen, G., Pavelsky, T., 2019. MERIT Hydro: A  
662 high-resolution global hydrography map based on latest topography datasets. *Water Resour. Res.*  
663 2019WR024873. <https://doi.org/10.1029/2019WR024873>  
664